Science Advances
AAAS

advances.sciencemag.org/cgi/content/full/5/5/eaav8141/DC1

Supplementary Materials for

Perovskite nanowire–block copolymer composites with digitally programmable polarization anisotropy

Nanjia Zhou, Yehonadav Bekenstein, Carissa N. Eisler, Dandan Zhang, Adam M. Schwartzberg, Peidong Yang, A. Paul Alivisatos*, Jennifer A. Lewis*

*Corresponding author. Email: paul.alivisatos@berkeley.edu (A.P.A.); jalewis@seas.harvard.edu (J.A.L.)

Published 31 May 2019, *Sci. Adv.* **5**, eaav8141 (2019)
DOI: 10.1126/sciadv.aav8141

This PDF file includes:

Fig. S1. Optical properties of $CsPbBr_3$ nanowires.
Fig. S2. Nanowire absorption spectra.
Fig. S3. Stability of $CsPb(Br_{0.2}I_{0.8})_3$ nanowires.
Fig. S4. Nanocomposite ink rheology.
Fig. S5. SAXS measurements of SIS block copolymer inks.
Fig. S6. TEM images of printed and cast nanocomposites.
Fig. S7. Polarization dependence of printed nanocomposite filaments composed of inks containing 50 wt % SIS with 0.05 wt % perovskite nanowires as a function of printing speed.
Fig. S8. Fourier imaging setup.
Fig. S9. Fourier images of printed SIS-$CsPbBr_3$ block copolymer nanocomposites.
Fig. S10. Measuring dipole alignment from Fourier images.
Fig. S11. Emission polarization of printed nanocomposite filaments.
Fig. S12. Five-layer photonic device showing “L-I-G-H-T” pattern imaged using polarized fluorescence microscopy along the *z* direction.
Fig. S13. Embedded 3D printing of perovskite nanowire ink in a transparent viscoplastic matrix housed within a cubic mold.
Fig. S14. Fluorescence images of printed pixel arrays showing polarization-dependent emission multiplexing using two nanowire composites printed in orthogonal directions.
Fig. S15. Schematics of different display operations presented in CIE 1931 diagram (Fig. 4D).
Table S1. Comparison of PLQY for different perovskite nanowires.
Table S2. Fluorescence stability of red-emitting $CsPb(Br_{0.2}I_{0.8})_3$ nanowires embedded in a polymer.
Table S3. Printing pressures used for patterning nanocomposite inks at varying nozzle sizes and print speeds.

Table S4. Hildebrand solubility and surface energies of species used to form nanocomposite inks.
Table S5. Comparison of different techniques for aligning semiconductor nanowires.
References (*37–44*)

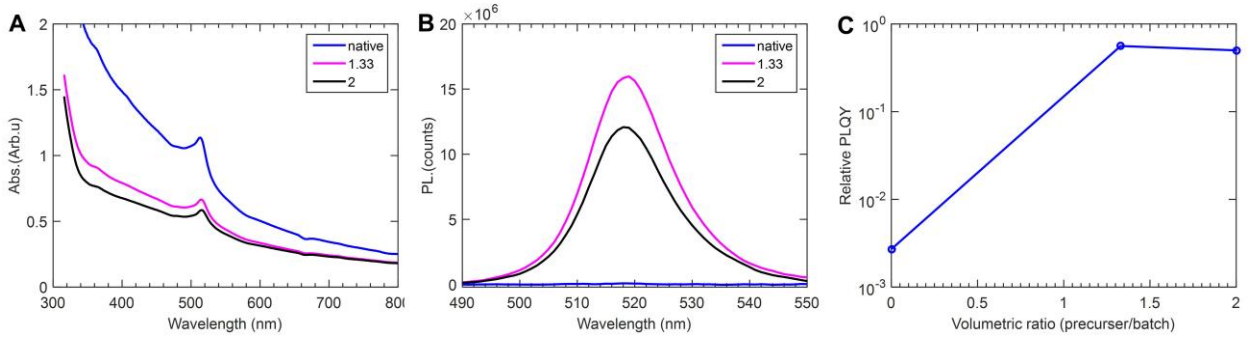

Fig. S1. Optical properties of $CsPbBr_3$ nanowires. (A) absorption spectra of $CsPbBr_3$ nanowires before and after surface modification, indicating that the overall position and shape of the absorption features (exciton) do not change. The different curves correspond to different volumetric ratios. **(B)** photoluminescence (PL) spectra of the native and treated nanowires, the number of counts increases dramatically after the surface treatment, due to surface reconstruction and the passivation of surface trapping states. **(C)** Logarithmic plot of the relative PL quantum yield (QY) volumetric ratios greater than 1.3 did not yield higher QY values.

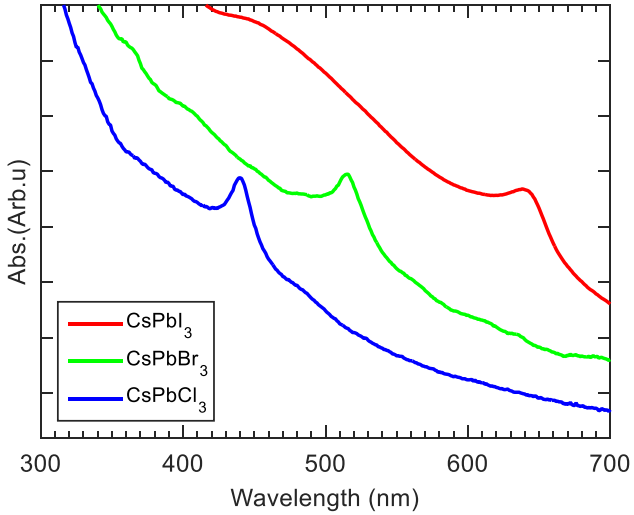

Fig. S2. Nanowire absorption spectra. Iodine-exchanged $CsPb(Br_{0.2}I_{0.8})_3$ nanowires exhibit red shifting of the emitted light due to narrowing of their electronic band gap, while chlorine-exchanged $CsPb(Br_{0.2}Cl_{0.8})_3$ nanowires exhibit blue shifting due to broadening of the electronic band gap compared to the as-synthesized $CsPbBr_3$ nanowires. [Note: The absorption peak shape, which is associated with the exciton, is maintained, yet shifted in the anion-exchanged nanowires.]

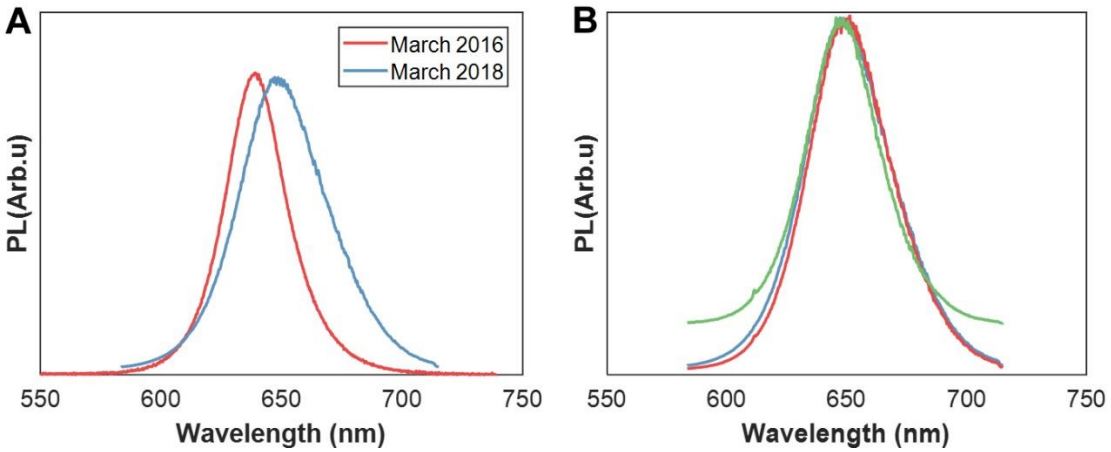

Fig. S3. Stability of $CsPb(Br_{0.2}I_{0.8})_3$ nanowires. (A) Photoluminescence spectra of α-$CsPb(Br_{0.2}I_{0.8})_3$ colloidal suspension of nanowires in toluene as measured with a fluorimeter on March 2016 (red curve). **(B)** Photoluminescence spectra of α-$CsPb(Br_{0.2}I_{0.8})_3$ colloidal nanowires embedded into a polymeric SEBS matrix, dried and stored in ambient conditions for two years. The blue curve is the spectra as measured with a confocal microscope on March 2018, $\lambda_{excitation}$ = 488 nm. In both measurements, the emission centered at 650nm suggests the perovskite nanowires are in the α-$CsPbI_3$ black phase rather than the yellow phase (~550 nm emission).

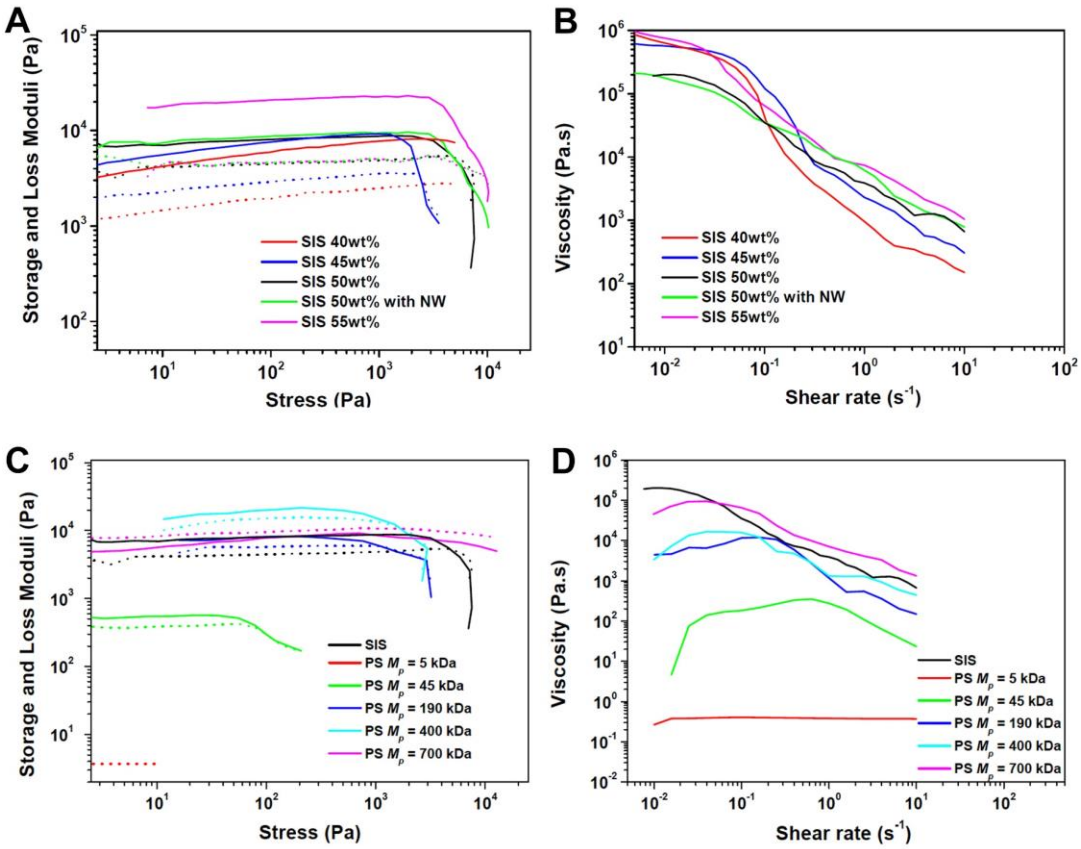

Fig. S4. Nanocomposite ink rheology. (A) and **(B)** Log-log plots of the storage and loss moduli as a function of shear stress and apparent viscosity as a function of shear rate, respectively, for nanocomposite inks composed of 40-55wt% SIS with or without $CsPbBr_3$ nanowires. **(C)** and **(D)** Log-log plots of the storage and loss moduli as a function of shear stress and apparent viscosity as a function of shear rate, respectively, for nanocomposite inks composed of 50wt% PS of varying molecular weights. [Note: The pure 50wt% SIS ink is included for comparison (black lines).] [Note: The storage and loss moduli are represented by the solid and dotted lines, respectively.]

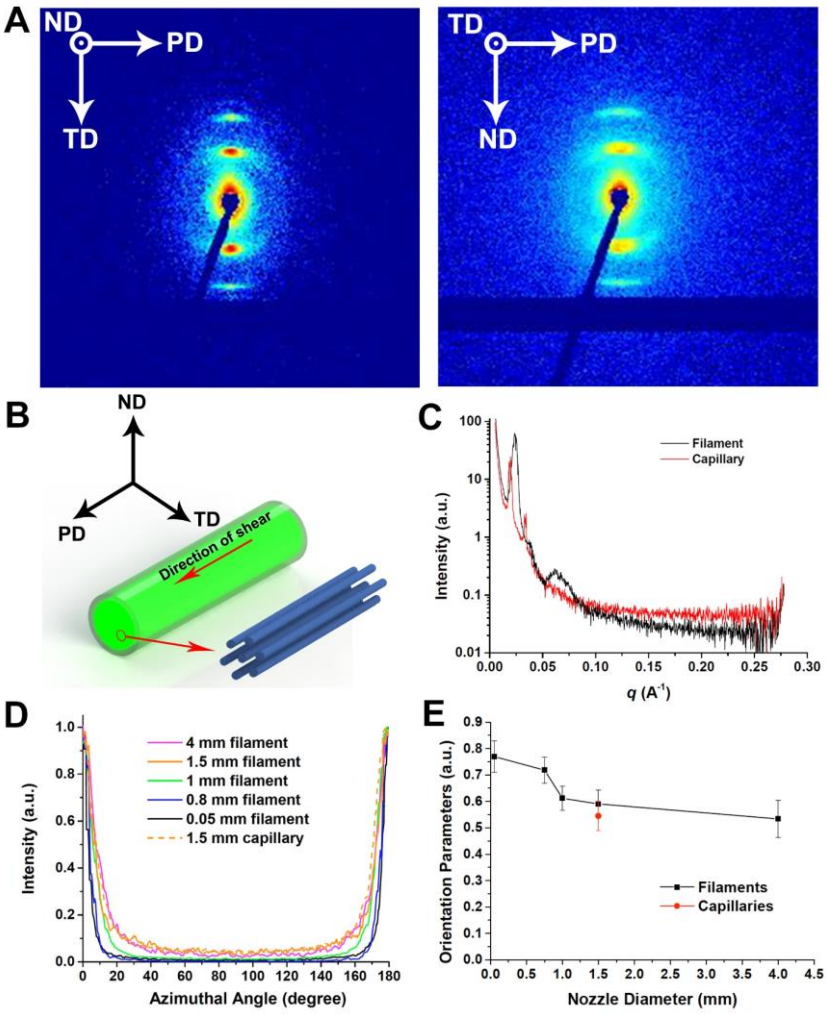

Fig. S5. SAXS measurements of SIS block copolymer inks. (A) 2D SAXS transmission patterns through the neutral direction (ND) (left) and the transverse direction (TD) (right) of an aliquot of SIS ink injected into a quartz capillary (1.5 mm diameter). [Note: The observed orientation is akin to SIS filaments printed using a 1 mm diameter nozzle (Fig. 1D).] **(B)** Schematic of SAXS measurement as a function of the printing direction. **(C)** SAXS 1D patterns of the SIS ink within a quartz capillary (ID = 1.5 mm) and a SIS filament printed using 1 mm nozzle. **(D)** Intensity distribution of 2D SAXS patterns along the azimuthal angle from 0 to 90° for SIS filaments printed using nozzles with diameters ranging from 0.05-4.0 mm as well as the SIS ink within a quartz capillary (1.5 mm diameter). **e**, Herman's orientation parameter[37] is calculated as

$$S = \frac{3\langle \cos^2 \emptyset \rangle - 1}{2}$$

where ϕ is the azimuthal angle and $\langle \cos^2 \phi \rangle$ is the average of $\cos^2\phi$ based on the average intensity at a given azimuthal angle, $I(\phi)$, calculated as

$$\langle \cos^2 \emptyset \rangle = \frac{\sum_{\emptyset=0}^{\pi/2} I(\emptyset) \sin \emptyset \cos^2 \emptyset}{\sum_{\emptyset=0}^{\pi/2} I(\emptyset) \sin \emptyset}$$

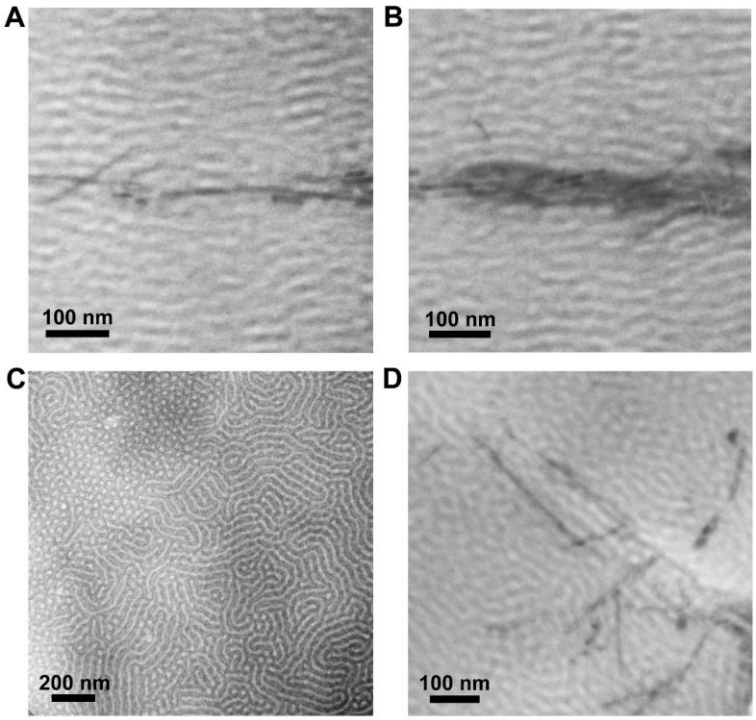

Fig. S6. TEM images of printed and cast nanocomposites. (A) isolated and **(B)** bundled $CsPbBr_3$ nanowires in printed nanocomposites (1 mm diameter nozzle); **(C)** pure SIS and **(D)** SIS-$CsPbBr_3$ composites (control samples) cast using dilute inks (2wt% in toluene). Samples are prepared using ultra-cryomicrotome. [Note: the PI nanophase separated domains appear electron-opaque due to selective OsO_4 staining[38].]

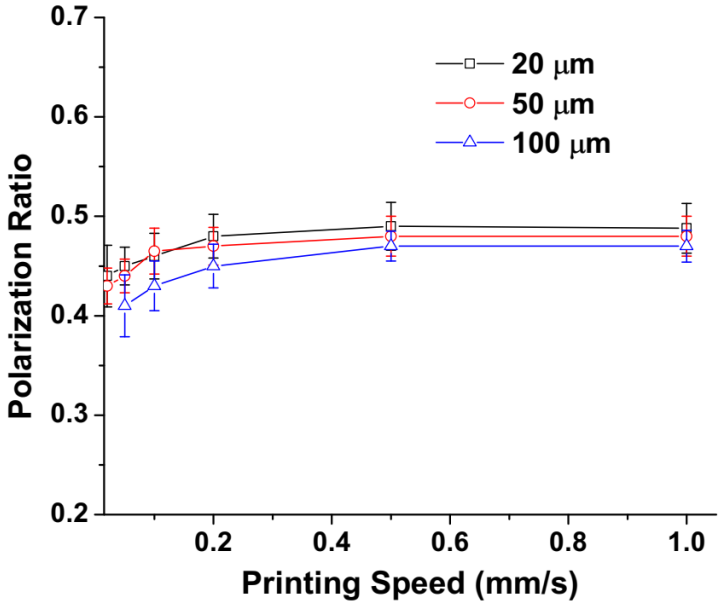

Fig. S7. Polarization dependence of printed nanocomposite filaments composed of inks containing 50 wt % SIS with 0.05 wt % perovskite nanowires as a function of printing

speed. The black, red, and blue data correspond to inner nozzle diameters of 20, 50 100 µm, respectively.

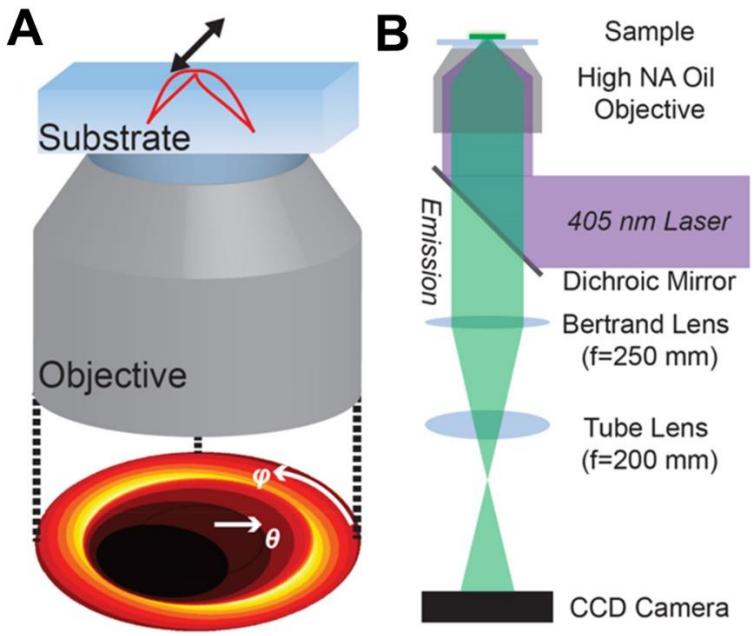

Fig. S8. Fourier imaging setup. The back focal plane of a microscope objective is imaged, while focused on a fluorescing luminophore[39]. This approach yields a polar image that is the 2D projection of the angular emission from the sample, where the polar angle (θ, relative to optical axis) follows the radius of the image and is limited by the NA of the microscope (here, NA=1.4) while the azimuthal angle (φ) follows the circumference. **(A)** Schematic of Fourier imaging setup adapted from[40], which shows the calculated pattern for dipole oriented at Θ = 45°, Φ = 45° at an air-glass (n = 1.5) interface. **(B)** Schematic of experimental setup based of design discussed in[32]. The tube lens and added Bertrand lens are a two-lens optical system that image the back focal plane of the objective.

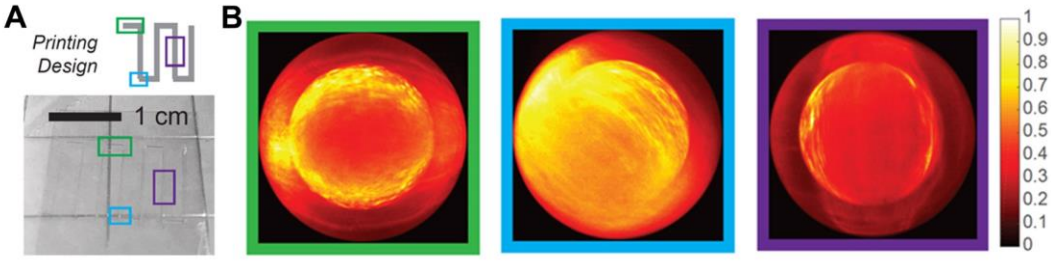

Fig. S9. Fourier images of printed SIS-$CsPbBr_3$ block copolymer nanocomposites. (A) Photograph and schematic of printed supramolecular nanocomposite on glass coverslip, printed in rectangular wave pattern. **(B)** Fourier images for printed supramolecular nanocomposite

filament at different positions. The axis of symmetry in the Fourier images tracks with the printing direction indicating that the nanowires are aligned along the printing direction.

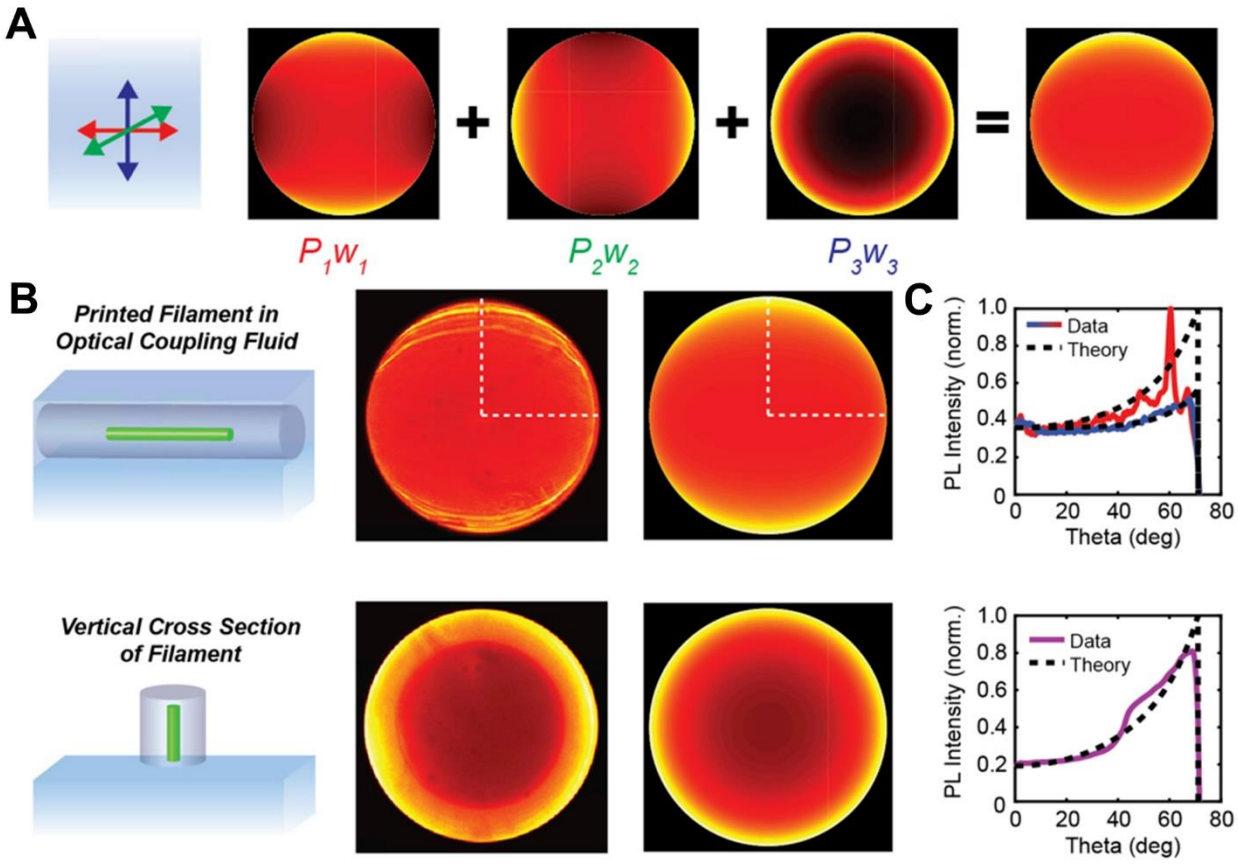

Fig. S10. Measuring dipole alignment from Fourier images. (A) Schematic of method used to calculate dipole alignment from Fourier images. The data is assumed to have contributions from three orthogonal dipoles with weights that sum to unity. The angular emission from each dipole is determined by calculating the radiative power of the dipole close to an interface. Each Fourier signal is weighted and summed to yield a final pattern. Theoretical profiles and the experimental data are compared to determine the best fit for multiple samples, including both horizontal filaments and vertical cross-sections of these filaments. In this example, the final signal is the result of 60% of dipoles aligned along the red axis and the remaining 40% dipoles split evenly along the blue and green axes. **(B)** Comparison of representative Fourier images to the theoretically generated BFP images. (Top) Horizontally printed 50 μm supramolecular nanocomposite filament submerged in oil to create nearly uniform optical environment. Symmetry about center horizontal axis is still observed for uniform optical environment, indicating that emission pattern is a result of aligned nanowires and not the shape of the filament. (Bottom) Cross section of filament (1 mm) oriented vertically on glass slide (thickness ~1 μm). **(C)** Profiles at φ = 0° and 90° were extracted and fit to theoretical curves for varying dipole contributions. Fits determined that 60% +/- 6% of dipoles are oriented along printing axis.[32,41]

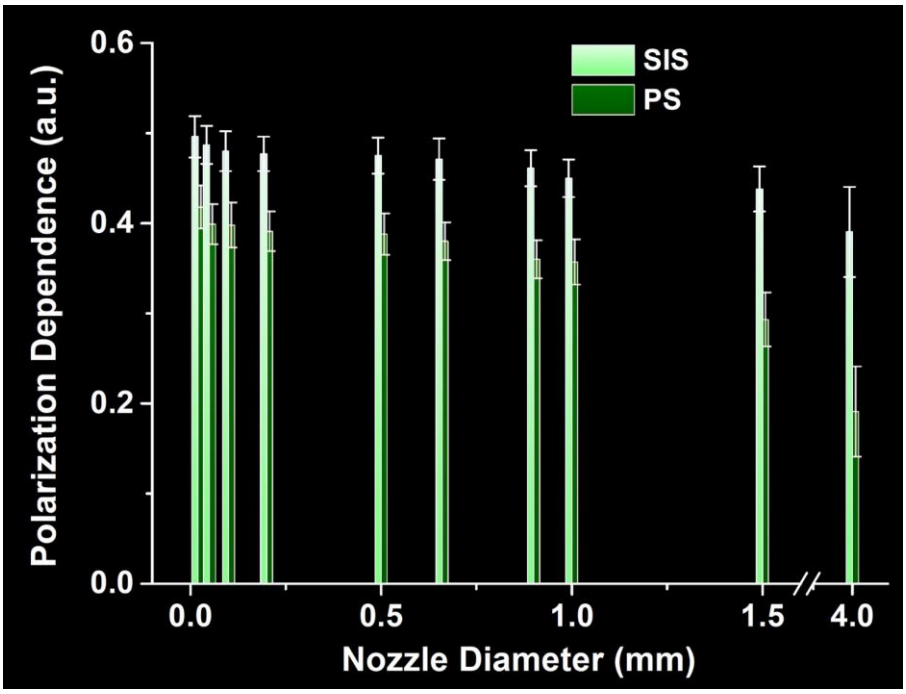

Fig. S11. Emission polarization of printed nanocomposite filaments. The polarization dependence of printed nanocomposite filaments composed of inks containing either 50 wt% SIS or pure PS with 0.05 wt% perovskite nanowires as a function of nozzle diameter. (Printing speed ~ 500 μm/s)

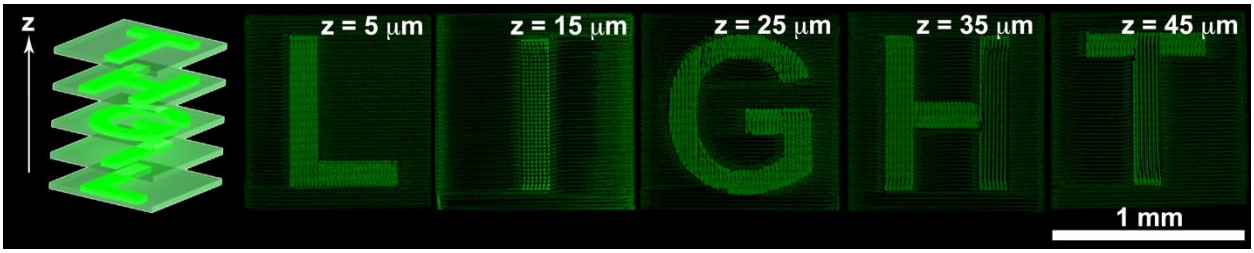

Fig. S12. Five-layer photonic device showing "L-I-G-H-T" pattern imaged using polarized fluorescence microscopy along the *z* direction. The five letters are printed parallel to the polarization direction.

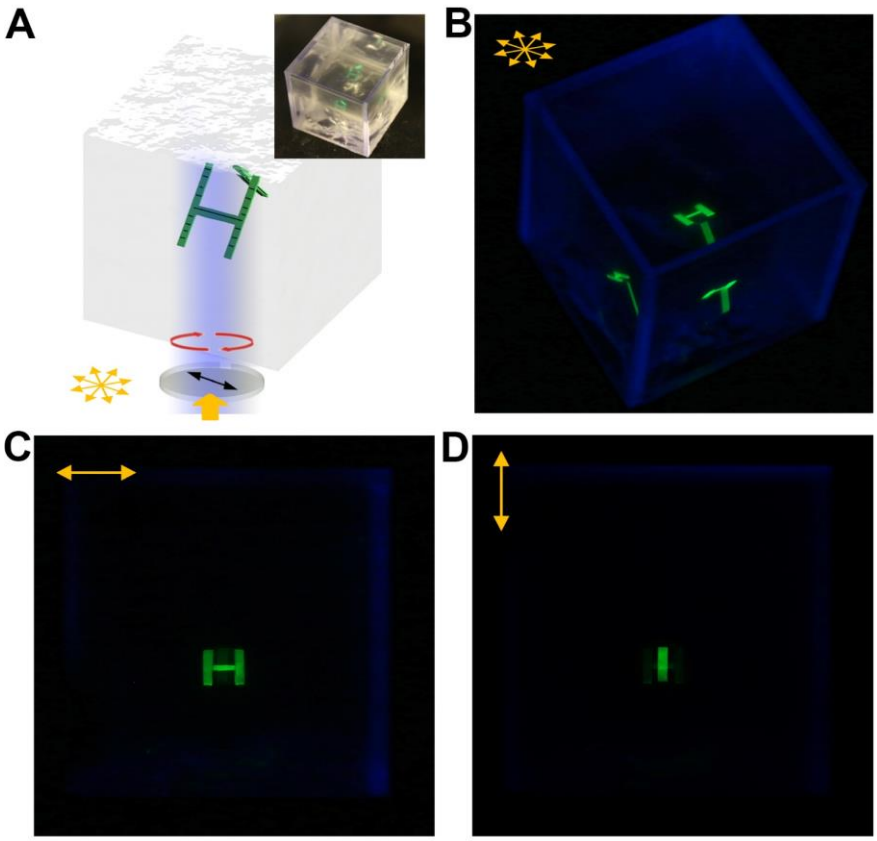

Fig. S13. Embedded 3D printing of perovskite nanowire ink in a transparent viscoplastic matrix housed within a cubic mold. (A) Schematics and photo (inset) showing "H" and "I" letter printed in different out-of-plane orientations. **(B)** Using non-polarized UV-light illumination, both letters are visible. **(C)** and **(D)** Using a polarizer and UV light illumination from the bottom of the cube, only the individual letters are visible.

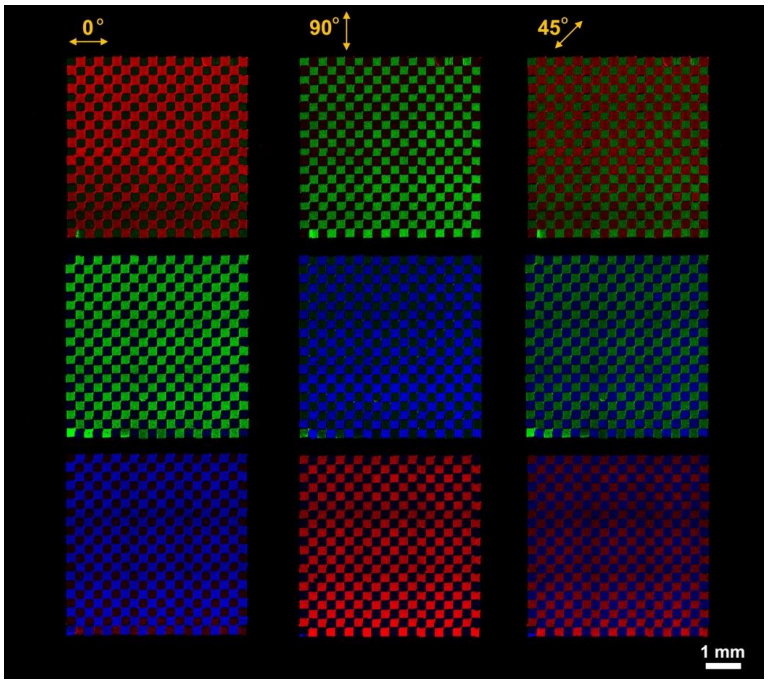

Fig. S14. Fluorescence images of printed pixel arrays showing polarization-dependent emission multiplexing using two nanowire composites printed in orthogonal directions. Top row: $CsPb(Br_{0.2}I_{0.8})_3$ + $CsPbBr_3$ (R+G); Middle row: $CsPbBr_3$ + $CsPb(Br_{0.2}Cl_{0.8})_3$ (G+B); Bottom row: $CsPb(Br_{0.2}Cl_{0.8})_3$ + $CsPb(Br_{0.2}I_{0.8})_3$ (B+R).

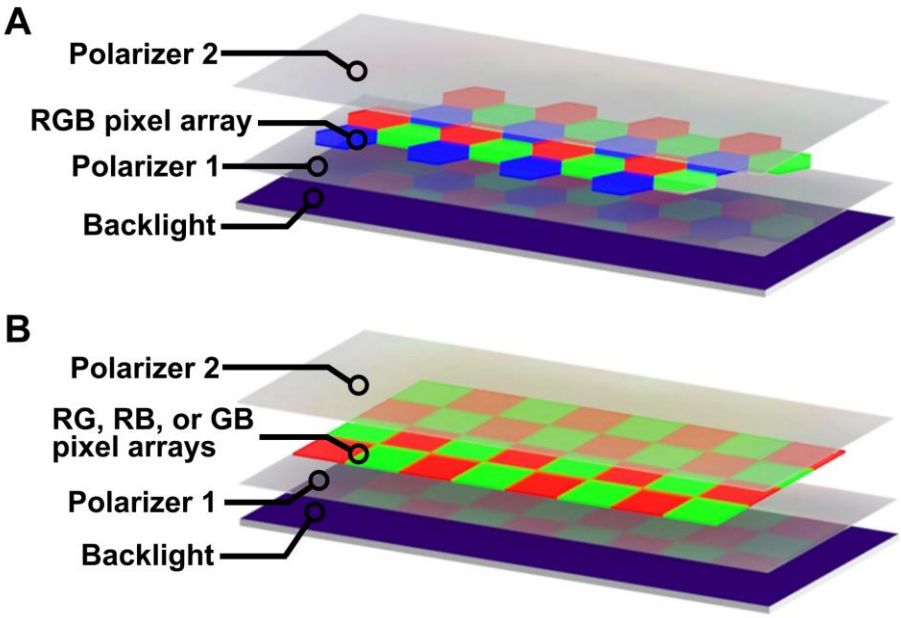

Fig. S15. Schematics of different display operations presented in CIE 1931 diagram (Fig. 4D). **(A)** Multiplexed RGB pixel arrays printed in three directions with 60° offset shown in Figs. 4B-C. A pair of polarizers are installed in the excitation and emission paths to enhance polarization dependence. The corresponding colors are represented in the CIE 1931 diagram as solid line, triangles. **(B)** Multiplexed RG, RB, and GB pixel arrays printed in two orthogonal directions shown above in fig. S14. The corresponding colors are represented in the CIE 1931 diagram using a dashed line and circular symbols. The intercepts of the three extrapolated lines representing RG, RB, and GB bicolor displays correspond to R, G, and B colors generated from pure nanowires (star symbols).

Table S1. Comparison of PLQY for different perovskite nanowires.

	Red emitting	**Green emitting**	**Blue emitting**
Composition	$CsPb(Br_{0.2}I_{0.8})_3$	$CsPbBr_3$	$CsPb(Br_{0.2}Cl_{0.8})_3$
PLQY after exchange to iodide and chloride	>95%	50% (as synthesized)	30%
QY when embedded in polymer matrix	85%	40%	NA*

*The absolute QY measurement system was altered between experiments on different perovskite nanowires, which hindered our ability to measure QY at these wavelengths.

Table S2. Fluorescence stability of red-emitting $CsPb(Br_{0.2}I_{0.8})_3$ nanowires embedded in a polymer.

Measurement	Emission peak (nm)	FWHM (nm)
March 2016	638.7	29.4
March 2018	648.7	41.9

Table S3. Printing pressures used for patterning nanocomposite inks at varying nozzle sizes and print speeds.

Printing speed / Nozzle size	20 µm/s	50 µm/s	100 µm/s	200 µm/s	500 µm/s	1 mm/s
20 µm	~15 psi	~40 psi	~65 psi	~150 psi	~200 psi	~320 psi
50 µm	~10 psi	~20 psi	~35 psi	~80 psi	~120 psi	~110 psi
100 µm	NA	~5 psi	~7 psi	~15 psi	~40 psi	~52 psi

Table S4. Hildebrand solubility and surface energies of species used to form nanocomposite inks.

	Hildebrand solubility δ, ($MPa^{1/2}$)	*Surface Energy (mJ/m^2)*
Oleic acid	15.6[42]	32.5[43]
Polyisoprene	16.7[44]	32[44]
Polystyrene	18.5[44]	40.7[44]

The Hildebrand solubility predicts a preferential segregation of nanowires in polyisoprene (PI) domains: i.e., $(\delta_{PS} - \delta_{oleic\ acid})^2$ = 8.41 MPa > 1.21 MPa = $(\delta_{PI} - \delta_{oleic\ acid})^2$]. This analysis is in good agreement with TEM images shown in Fig. 1F, where nanowires are predominantly observed in PI domains (dark). We note that Mayeda et al.[44] found that the ligands furthest away from nanoparticle cores control their solubility. Hence, in our case, 9-octadecene would give rise to a lower Hildebrand solubility, leading to preferential segregation of nanowires in PI domains.

Table S5. Comparison of different techniques for aligning semiconductor nanowires.

	Electrospinning	**Photoalignment**	**Direct Ink Writing**
Degree of alignment (DOP)	0.6-0.74	~0.8	0.48
Minimum feature size	~50 nm	NA	~10 um
Printed geometry	2D films	2D films	Fully customizable 3D structures.
Voxelated with different NR orientations	Limited to unidirectional alignment	Yes	Yes
Multiple-layer films with same of different NR	No	Limited to 3 layers	Yes
Pattern multiple materials in different orientations in the same plane (i.e. for polarized color filter)	No	No	Yes
Out-of-plane alignment capability	No	No	Yes